Supplementary Materials and Methods

Genetics. Flies expressing the following transgenes were used in this study: *chaoptin* (*chp*)-*Gal4* (a generous gift from S. L. Zipursky, University of California, Los Angeles, CA), *actin* (*act*)-*Gal4* (Bloomington *Drosophila* Stock Center), *PM181-Gal4* (Lee et al., 2001), *UAS-wnd* (*wnd^{OE}*; Collins et al., 2006), *UAS-Bsk^{DN}* (*JNK^{DN}*; Weber et al., 2000, Bossuyt et al., 2009), *UAS-mCD8-ChRFP* (Bloomington *Drosophila* Stock Center), *UAS-Dcr-2* (Dietz *et al* 2007), *UAS-mCD8-GFP* (Lee and Luo, 1999), *UAS-EB1-GFP* (Rolls et al., 2007), 20C11-FLP (Chen et al., 2014); brp-FSF-GFP (Chen et al., 2014), and UAS-FSF-tdTomato-myr (Chen et al., 2014). *UAS-RNAi* lines from the Vienna *Drosophila* Resource Center (Dietz et al., 2007) were used to knock down expression of Ttk69 (#101980) and Babo (#106092), and a *UAS-RNAi* stock from the Transgenic RNAi Resource Project was used to knockdown Hiw (Ni et al., 2009; Bloomington *Drosophila* Stock Center # 28031).

"wild type" animals in Fig. 1, 2G, 3, 5A, S1, S2C, S3C and S3I were *UAS-Dcr-2/+;;chp-Gal4*, *UAS-EB1-GFP/+* or *UAS-Dcr-2/Y;;chp-Gal4*, *UAS-EB1-GFP/+.*

"wild type" animals in Fig. 2A-F were *UAS-Dcr-2/+; UAS-mCD8-GFP/+; chp-Gal4/+* or *UAS-Dcr-2/Y; UAS-mCD8-GFP/+; Chp-Gal4/+.*

"wild type" animals in Fig. 5B and S3A-B were *UAS-Dcr-2/Y;;chp-Gal4*, *UAS-EB1-GFP/+.*

"wild type" animals in Fig. S2A-A'' were *+/Y;; UAS-mCD8-GFP, PM181-Gal4/+.*

"*wild type"* animals in Fig. 6, 7 were *UAS-Dcr-2;; chp-Gal4, UAS-EB1-GFP*

We used the *hiw* loss-of-function alleles *hiw$^{\Delta N}$*, *hiw$^{\Delta C}$* and *hiw^{ND8}* (Wu et al., 2005) and found that *hiw* mutant animals of genotype *hiw$^{\Delta N}$/Y*, *hiw$^{\Delta C}$/Y*, *hiw$^{\Delta N}$/ hiw$^{\Delta C}$,* or *hiw^{ND8}/hiw$^{\Delta N}$* had indistinguishable R7 phenotypes (data not shown).

'*hiw*'' mutant animals in Fig.1, 3, 5, S1 and S3 were *hiw$^{\Delta N}$/Y; chp-Gal4, UAS-EB1-GFP/+* or *hiw$^{\Delta C}$/Y; chp-Gal4, UAS-EB1-GFP/+*

"*hiw*'' mutant animals in Fig. 2 were *hiw$^{\Delta N}$/Y; UAS-mCD8-GFP; chp-Gal4/+*

"*hiw*'' mutant animals in Fig. S2 were *hiw$^{\Delta N}$/Y; UAS-mC8GFP, PM181-Gal4/+*.

"JNK^{DN}" animals in Fig. 1, 2, 3, 5A S2 and S3 were *UAS-Dcr-2/+;; chp-Gal4*, *UAS-EB1-GFP/UAS-Bsk^{DN}* or *UAS-Dcr-2/Y;;chp-Gal4*, *UAS-EB1-GFP/ UAS-Bsk^{DN}.*

"wnd" mutant animals in Fig. 1, 2, and S1 were *UAS-Dcr-2/w; UAS-mCD8-GFP/+; chp-Gal4, wnd^{1}/wnd^{3}* or *w/Y; UAS-mCD8-GFP/+; chp-Gal4, wnd^{1}/wnd^{3}*. This allelic combination has previously been reported to be a protein null (Wu et al., 2007).

"*hiw, wnd"* mutant animals in Fig 2D-F were *hiw$^{\Delta N}$; UAS-mCD8-GFP/+; chp-Gal4, wnd^{1}/wnd^{3}*

"*wnd^{OE}*" animals in Fig. 2G, 3, and S2 were *w; UAS-wnd/UAS-mCD8-RFP; chp-Gal4, UAS-EB1-GFP/+*or *w/Y; UAS-wnd/UAS-mCD8-RFP; chp-Gal4, UAS-EB1-GFP/+*.

"*wnd^{OE}*" animals in Fig. 4K-L' were *w; 20C11-FLP/UAS-wnd; chp-Gal4/brp-FSF-GFP, UAS-FSF-tdTomato*.

"*wnd^{OE}*" animals in Fig. 5A were *UAS-Dcr-2/w; UAS-wnd/+; chp-Gal4, UAS-EB1-GFP/+* or *UAS-Dcr-2/Y UAS-wnd/+; chp-Gal4, UAS-EB1-GFP/+*.

"*wnd^{OE}*" animals in Fig. 5B were *UAS-Dcr-2/Y UAS-wnd/+; chp-Gal4, UAS-EB1-GFP/+*.

"*wnd^{OE}"* animals in Fig. 6, 7 were *UAS-Dcr-2/w; UAS-wnd; chp-Gal4, UAS-EB1-GFP*

"wnd^{OE}; JNK^{DN}" animals in Fig 3G,H and S2 were *w; UAS-wnd/+; chp-Gal4, UAS-EB1-GFP/UAS-Bsk^{DN}* or *w/Y; UAS-wnd/+; chp-Gal4, UAS-EB1-GFP/UAS-Bsk^{DN}*

"hiwRNAi" animals in Fig. 5 were *UAS-Dcr-2/w; UAS-hiwRNAi/+; chp-Gal4, UAS-EB1-GFP/+* or *UAS-Dcr-2/Y; UAS-hiwRNAi/+; chp-Gal4, UAS-EB1-GFP/+*

"*ttkRNAi*" animals in Fig. 5A and S3F and S3I were *UAS-Dcr-2/Y; UAS-ttkRNAi/+; chp-Gal4, UAS-EB1-GFP/+* or *UAS-Dcr-2/+; UAS-ttkRNAi/+; chp-Gal4, UAS-EB1-GFP/+*.

"*ttkRNAI"* animals in Fig. 5A and S3F also included *w/Y; UAS-ttkRNAi/+; chp-Gal4, UAS-EB1-GFP/ UAS-Dcr-2*

"*ttkRNAi"* animals in Fig. S3I also included *UAS-Dcr-2; UAS-mCD8-GFP/UAS-ttkRNAi; chp-Gal4/+*

"*ttkRNAi*" animals in Fig. 5B, and S3B were *UAS-Dcr-2/Y; UAS-ttkRNAi/+; chp-Gal4, UAS-EB1-GFP/+.*

"*ttkRNAi"* animals in Fig. 6, 7 were *UAS-Dcr-2; UAS-ttkRNAi/+; chp-Gal4, UAS-EB1-GFP.*

"hiw, ttkRNAi" animals in Fig. 5A, S3G, I were *hiw$^{\Delta N}$; UAS-ttkRNAi/+; chp-Gal4, UAS-EB1-GFP/UAS-Dcr-2*

"ttkRNAi; JNK^{DN}" animals in Fig. 5 and S3 were *UAS-Dcr-2/Y; UAS-ttkRNAi/+; chp-Gal4, UAS-EB1-GFP/UAS-Bsk^{DN}* or *UAS-Dcr-2/w; UAS-ttkRNAi/+; chp-Gal4, UAS-EB1-GFP/UAS-Bsk^{DN}*.

"ttkRNAi, hiwRNAi" animals in Fig. 5 were *UAS-Dcr-2/w:; ttkRNAi/+; chp-Gal4, UAS-EB1-GFP/UAS-hiwRNAi* or *UAS-Dcr-2/Y:; ttkRNAi/+; chp-Gal4, UAS-EB1-GFP/UAS-hiwRNAi*

"*baboRNAi*" animals in Fig. 6 and 7 were *UAS-Dcr-2/Y*; *UAS-baboRNAi/+; chp-Gal4, UAS-EB1-GFP* or *UAS-Dcr-2/w*; *UAS-baboRNAi/+; chp-Gal4, UAS-EB1-GFP.*

"*ttkRNAi, wnd"* animals in Fig S3I were *UAS-Dcr-2/w; UAS-mCD8-GFP/UAS-ttkRNAi; chp-Gal4, wnd^{1}/wnd^{3}* or *UAS-Dcr-2/Y; UAS-mCD8-GFP/UAS-ttkRNAi; chp-Gal4, wnd^{1}/wnd^{3}*

In Fig. 4, homozygous wild type (*FRT82*), *ttk69* mutant (*ttk^{1e11}*; Xiong and Montell, 1993), or *UAS-wnd* overexpressing R7 clones were generated and labeled using *GMR-FLP* and MARCM (mosaic analysis with a repressible cell marker; Lee and Luo, 1999; Lee et al., 2001).

"wild type" animals in Fig. 4 were *GMR-FLP/Y*; *act-Gal4, UAS-mCD8-GFP/+; FRT82/FRT82, tub-Gal80* or *GMR-FLP/y, w*; *act-Gal4, UAS-mCD8-GFP/+; FRT82/FRT82, tub-Gal80*.

"*ttk69 mutant"* animals in Fig. 4 and S3I were *GMR-FLP/Y*; *act-Gal4, UAS-mCD8-GFP/+; FRT82, ttk^{1e11}/FRT82, tub-Gal80* or *GMR-FLP/y, w*; *act-Gal4, UAS-mCD8-GFP/+; FRT82, ttk^{1e11}/FRT82, tub-Gal80*.

"*wnd^{OE}*" animals in Fig. 4B,C,F,I were *GMR-FLP/Y*; *act-Gal4, UAS-mCD8-GFP/UAS-wnd; FRT82/FRT82, tub-Gal80* or *GMR-FLP/y, w*; *act-Gal4, UAS-mCD8-GFP/UAS-wnd; FRT82/FRT82, tub-Gal80*.

"*JNK^{DN}, ttk69"* animals in Fig. S3I were *GMR-FLP/UAS-Bsk^{DN}; act-Gal4, UAS-mCD8-GFP/+; FRT82, gal80/FRT82, ttk^{1e11}*.

Antibodies. We used the following antibodies: mouse anti-Chp (24B10; 1:200) from the Developmental Studies Hybridoma Bank; rabbit anti-Wnd (A3-1,2; 1:300; Collins et al., 2006), a generous gift from C. Collins; chicken anti-GFP (1:1000) from Abcam, rabbit anti-GFP (1:5000) and all secondary antibodies (goat IgG coupled to Alexa Fluor 488, Alexa Fluor 555, or AlexFluor 633; 1:250) from Life Technologies.

Quantification of circularity. R7 growth cone circularity was measured by acquiring shape descriptors of R7 growth cone ROIs using ImageJ software. Within each brain, 20 clearly-identifiable R7 growth cones were traced in an approximately 10 µm-thick z-stack. Circularity was defined as: circularity = $4\pi(\text{area}/\text{perimeter}^2)$. Circularity =1 therefore indicates a perfect circle, and smaller values indicate irregular or elongated shapes.

Quantification of the frequency of R7s extending processes beyond or within their target layer. Within each brain, this frequency was determined by counting the number of R7 axon terminals exhibiting the phenotype in an approximately 10 µm-thick z-stack of the optic lobe and dividing by the total number of R7 terminals in the stack. A typical 10 µm-thick z-stack contained approximately 70 R7 terminals.

Localization of Brp-GFP puncta. We used *20C11-FLP* and the STaR technique to cause R7s to express Brp-GFP at endogenous levels. We then identified Brp-GFP puncta within R7 axons as regions that co-stained with anti-GFP and anti-Chp antibodies. This antibody staining also results in a non-specific background haze that allows optic lobe neuropil to be distinguished from cortex. We could therefore identify the medulla, lobula, and lobula plate neuropils based on position and shape (Meinertzhagen and Hanson, 1993). In R7s that overexpress Wnd, most Brp-GFP

puncta localize to the M6 layer. Within processes that Wnd-overexpressing R7s extend beyond the M6 layer, Brp-GFP puncta specifically localize to the edge of the medulla neuropil just beyond layer M10 or to a region between the lobula and lobula plate that we did not attempt to define further.

qPCR Primers. The following primer sequences (5' → 3') were used for qPCR in this study. Rpl32 Forward: CTAAGCTGTCGCACAAATGGC, Rpl32 Reverse: TTGCGCTTCTTGGAGGAGAC, Wnd Forward: GGCAGGCTAAAGAACGAGACT, Wnd Reverse: CCAAGCGGGACGGTAACAT, Faf Forward: GTGGACAGCACCATCACAATAG, and Faf Reverse: CACAAGGATACAGTGGTGGATGT

Supplementary Figures

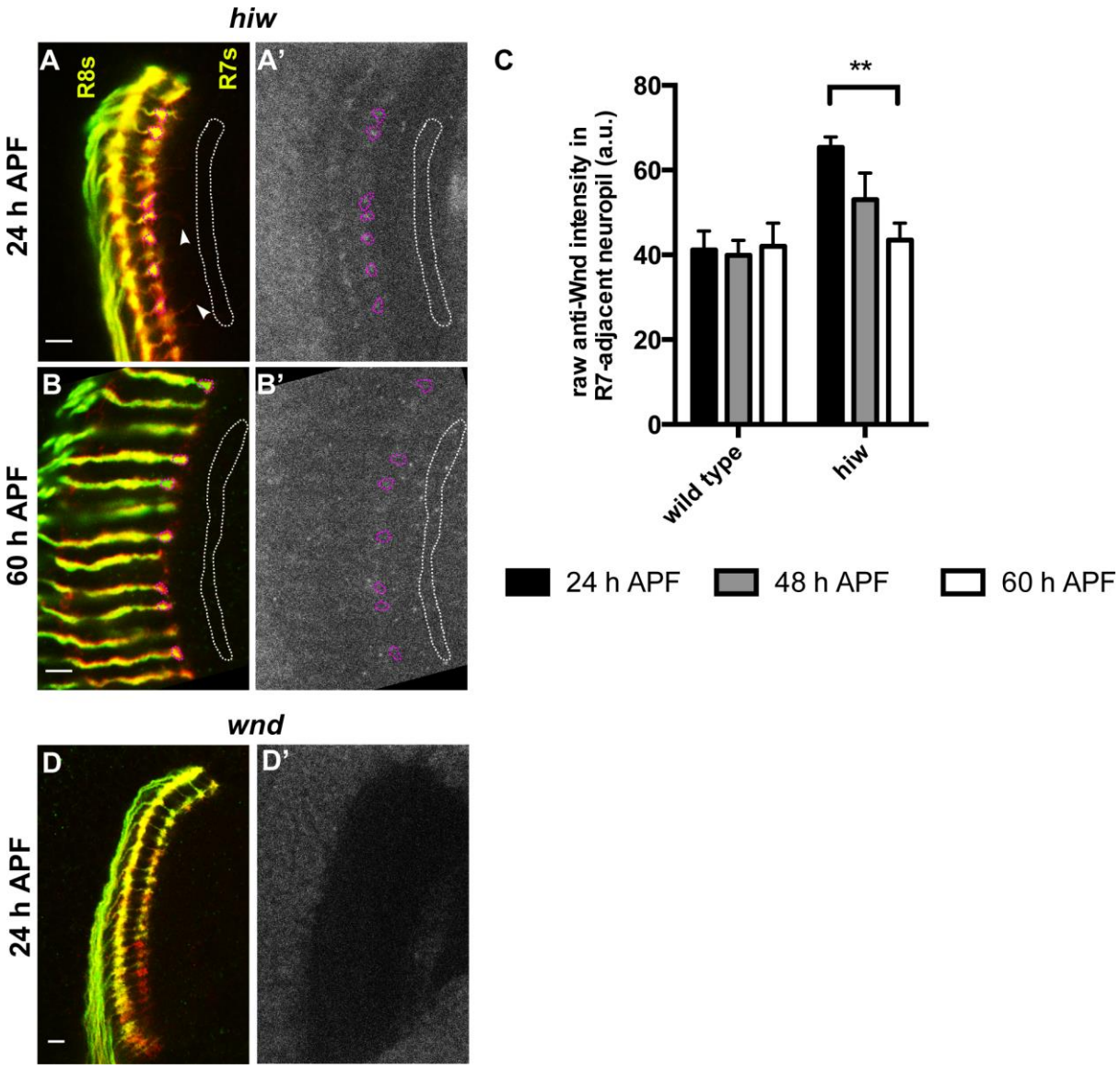

Fig. S1. Details on how anti-Wnd staining in R7 growth cones was quantified. (A-B') Exemplar *hiw* mutant pupal medullas (25°C) in which R7 and R8 are labeled with (A,B) *chp-Gal4, UAS-EB1-GFP* (green) and anti-Chp (red) and (A',B') anti-Wnd. Abnormal R7 processes are indicated by arrowheads. In all genotypes, at both 24 (A') and 60 h APF (B'), anti-Wnd staining was quantified by using anti-Chp alone to trace R7 growth cones (e.g., magenta dotted lines in A-B') and an adjacent region of neuropil (e.g., white dotted lines in A-B'). To calculate "% increase of anti-Wnd over background fluorescence" in Fig. 1E and Fig. 5A, the level of anti-Wnd staining within each R7 tracing was measured and divided by the average level of anti-Wnd staining within the adjacent region. This normalization decreased the variability caused by stochastic differences in antibody staining efficiencies among brains. (C) Quantification of average raw fluorescence intensities within the R7-adjacent

neuropil (e.g., white dotted lines in A-B') in wild-type and *hiw* mutant brains over time. n= brains, error bars represent SEM. n= 14, 19, 16, 10, 12, and 17, respectively. There is no significant change in anti-Wnd staining in this region in wild type; our use of this region to normalize the anti-Wnd staining within R7 growth cones therefore does not confer or obscure temporal differences in wild-type R7s. There is a significant decrease in anti-Wnd staining in this region in *hiw* mutant animals between 24 and 60 h APF, suggesting that a temporal, Hiw-independent mechanism might also repress Wnd in medulla axons. Our use of this region to normalize the anti-Wnd staining within *hiw* mutant R7 growth cones may therefore cause us to underestimate the strength of the Hiw-independent repression of Wnd that occurs in R7 growth cones.(D,D') *wnd* mutant pupal medulla (25°C) in which R7 and R8 are labeled with (D,E) *chp-Gal4, UAS-mCD8-GFP* (green) and anti-Chp (red) and (D') anti-Wnd. There is little anti-Wnd staining in the medulla neuropil of *wnd* protein-null mutants (quantified in Fig.1E); however, the surrounding cortex (which contains the cell bodies of medullar neurons and glia) stains brightly. We conclude that the cortical staining in this and other genotypes is therefore at least partly non-specific and does not accurately reflect Wnd levels.

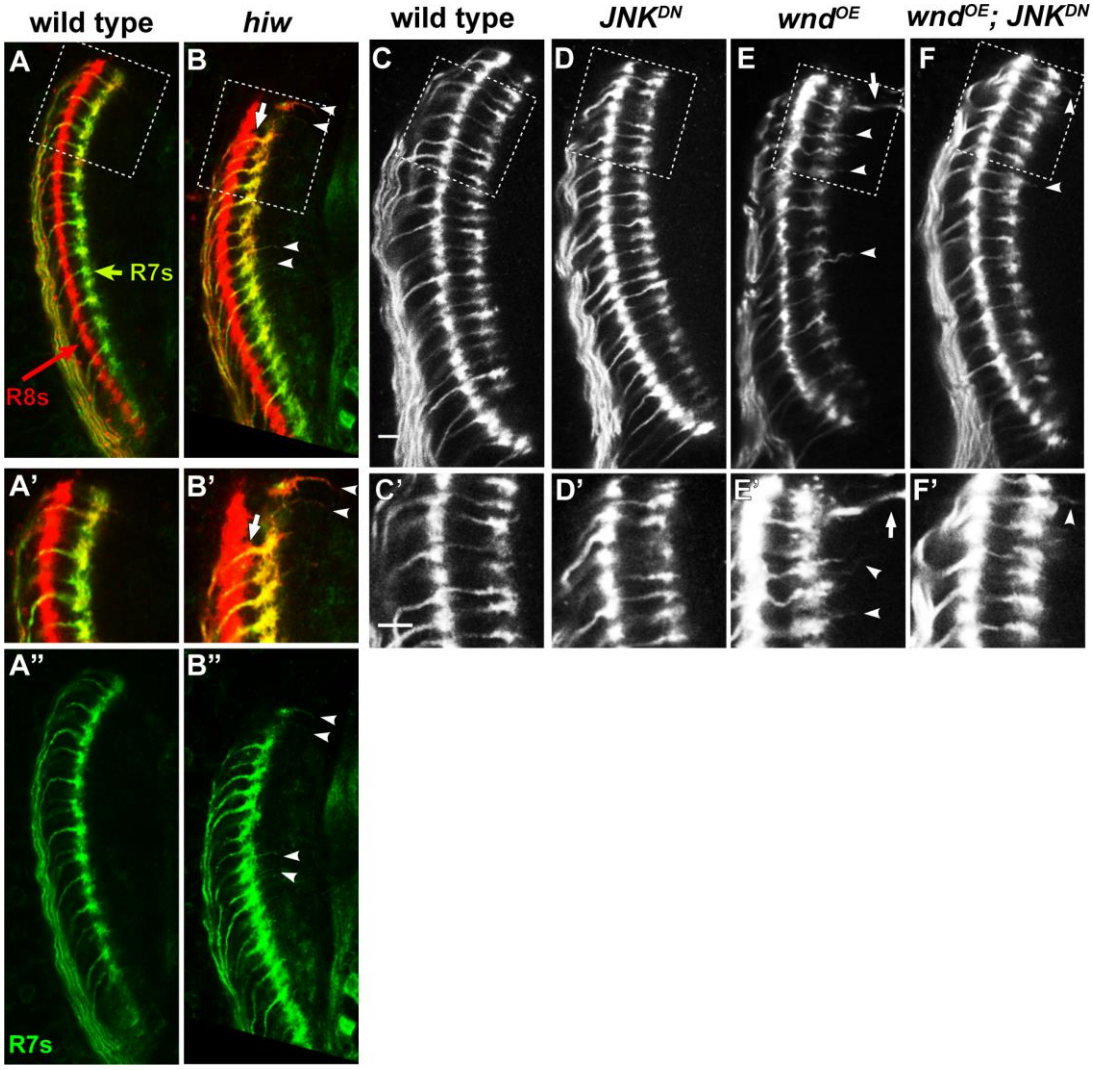

Fig. S2. Wnd disrupts layer-specific R7 growth cone halting through JNK.
(A-B") 24 h APF pupal medullas (25°C) in which R7 axons are specifically labeled with *PM181-Gal4, UAS-mCD8-GFP* (green), and both R7 and R8 axons are labeled with anti-Chp (red). A' and B' are enlargements of the boxed regions in A and B with brightness enhanced so that thin growth cone processes are visible. The R7-specific labeling confirms that it is the R7s in *hiw* mutants that extend processes beyond their target layer (arrowheads) and that it is not R7s that occasionally terminate between the R8 and R7 target layers (arrow in B and B' pointing to growth cone between R8 and R7 target layers that is stained red but not green).
(C-F'), 24 h APF pupal medullas (29ºC), in which R7 and R8 axons are labeled with *chp-Gal4, UAS-EB1-GFP* (white) . Scale bars are 5 µm. (C'-F') are enlargements of the boxed regions in (C-F) with enhanced brightness. R7 growth cones expressing dominant-negative JNK (JNK^{DN}; D,D') are indistinguishable from wild type (C,C'). R7 growth cones expressing wild-type Wnd (Wnd^{OE}; E,E') extend processes beyond their target layer (arrowheads); these processes resemble those in *hiw* mutants but sometimes extend deeper into the optic lobe (arrows). Co-expressing JNK^{DN} with wild-type Wnd almost completely ameliorates this defect (F,F', arrowheads indicate some remaining abnormal processes). These phenotypes are quantified in Fig. 2G.

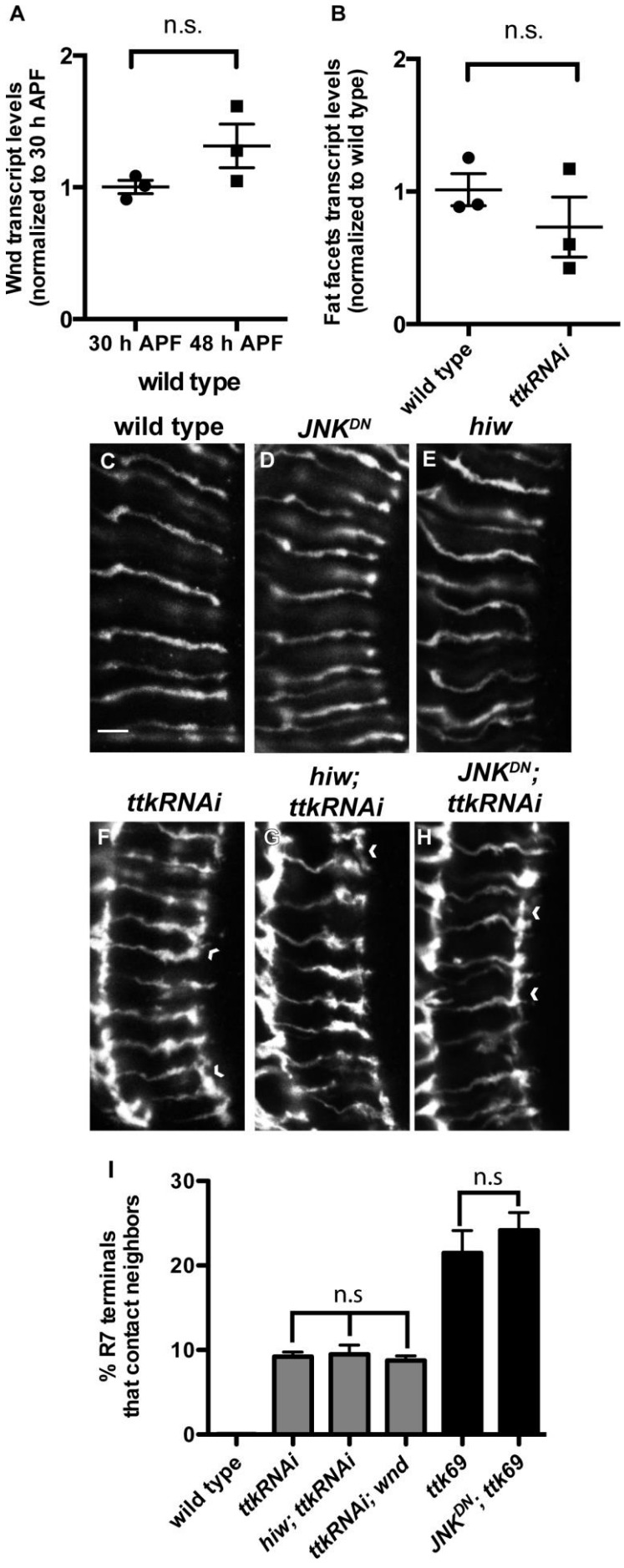

Fig. S3. Ttk69 regulates Wnd protein expression indirectly and regulates additional pathways to promote R7 growth cone remodeling.
(A,B) Quantifications of transcript levels measured by qRT-PCR on RNA extracted from dissected retinas. n= 3 biological replicates, and error bars represent SEM. (A) There is no detectable change in *wnd* mRNA levels as R7 growth cone remodeling progresses. (B) Loss of *ttk69* from R neurons does not detectably increase *fat facets* (*faf*) mRNA levels. (C-H) 48 h APF pupal medullas (29°C) in which R7 and R8 axons are labeled with *chp-Gal4, UAS-EB1-GFP*. Scale bars are 5 µm. (I) Quantification of the frequency with which R7 axon terminals contact their neighbors. n=brains and error bars represent SEM. n.s. not significant based on a pairwise two-tailed t-test. n=17, 22, 11, 10, 5, and 9, respectively. Wild-type (C), JNK^{DN}-expressing (D), and *hiw* mutant R7 axon terminals (E) are indistinguishable. The frequency with which R7s expressing *ttkRNAi* contact their neighbors (F; chevrons) is not increased by additional loss of *hiw* (G,I). And loss of *JNK* (caused by expressing JNK^{DN}; H) or *wnd* (I) from *ttkRNAi*-expressing R7s does not ameliorate this defect. Similarly, disrupting *JNK* in *GMR-FLP*-generated *ttk69* mutant R7s (by causing them to express JNK^{DN}) does not ameliorate this defect. Note that contacts between individually-labeled *GMR-FLP*-generated *ttk69* mutant R7 axon terminals and their neighbors are easier to score than contacts among uniformly labeled R7 axon terminals, so the frequency of this defect is scored as much higher in the former situation.

Multimedia

Spinning disk confocal movies, each spanning 30 minutes of real time, sped up 300x (10 frames were collected every 30 seconds but are here presented at 1 frame/second). See Methods for imaging conditions.

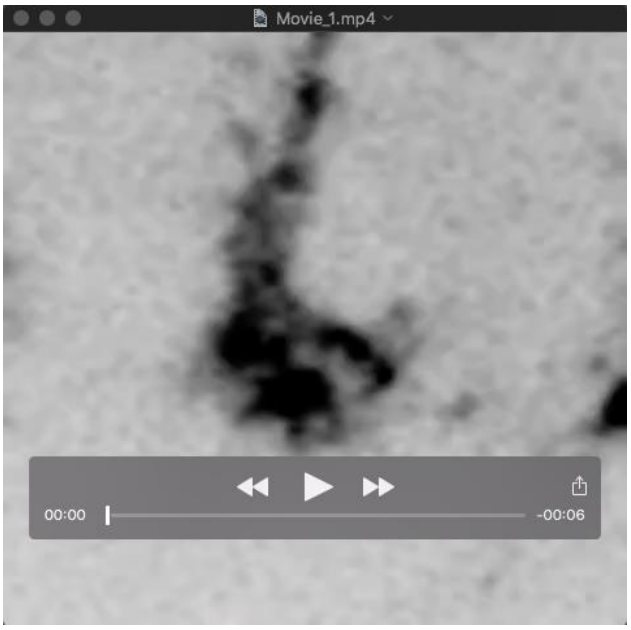

Movie 1. Representative wild-type R7 axon terminal at 40 h APF.

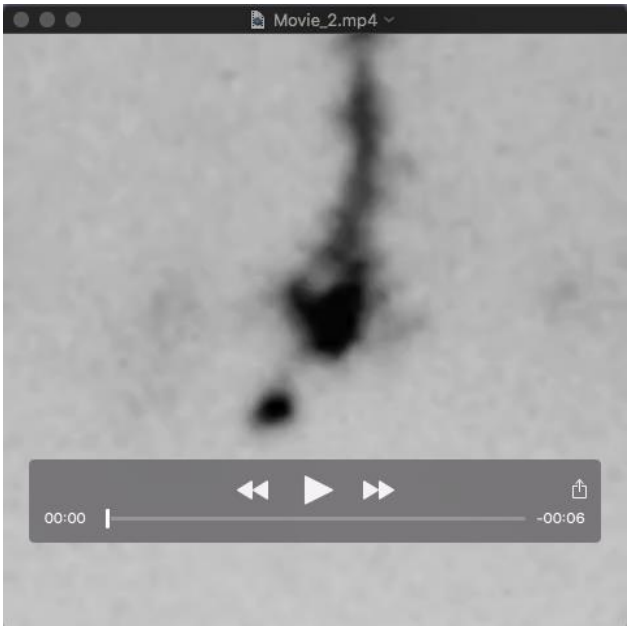

Movie 2. Representative wild-type R7 axon terminal at 48 h APF. The average extension and retraction velocities of processes are reduced compared to 40 h APF.

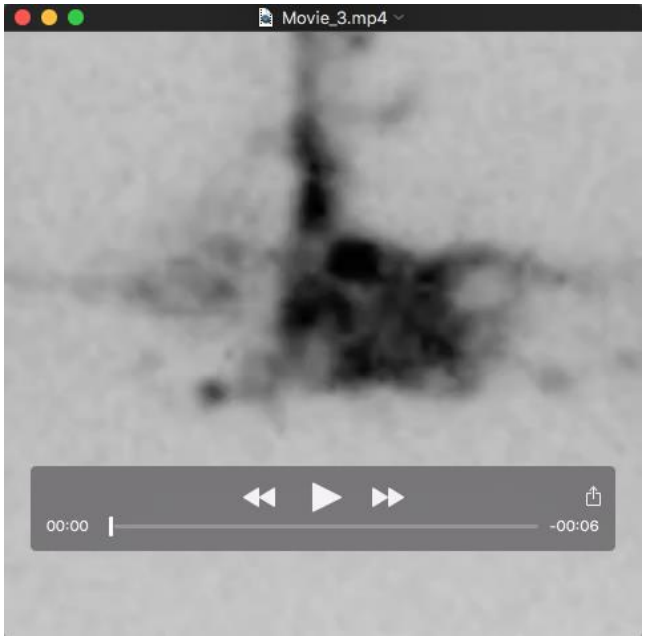

Movie 3. Representative *wnd*^{OE} R7 axon terminal at 40 h APF. The average extension and retraction velocities of processes are indistinguishable from those in wild type at 40 h APF.

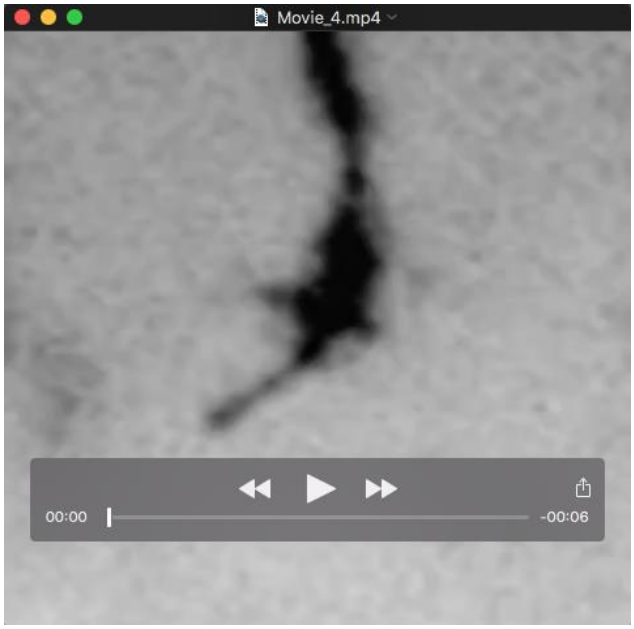

Movie 4. Representative *wnd*^{OE} R7 axon terminal at 48 h APF. The average extension and retraction velocities of processes are greater than those in wild type at 48 h APF.

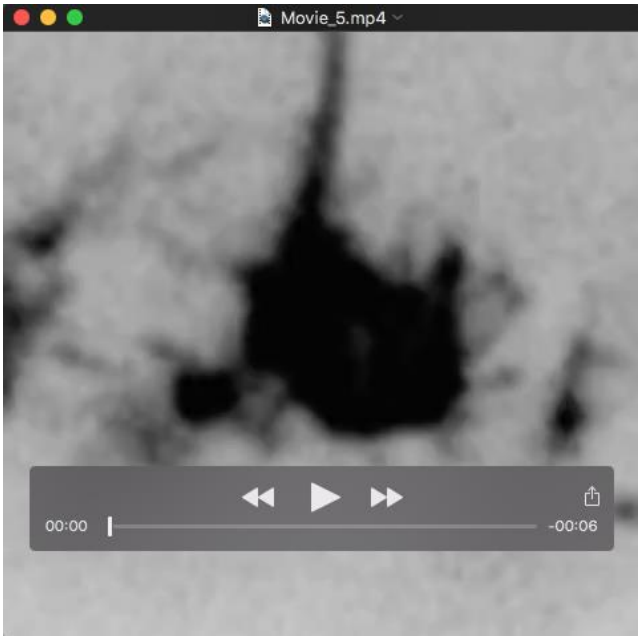

Movie 5. Representative *ttkRNAi*-expressing R7 axon terminal at 40 h APF. The average extension and retraction velocities of processes are indistinguishable from those in wild type at 40 h APF.

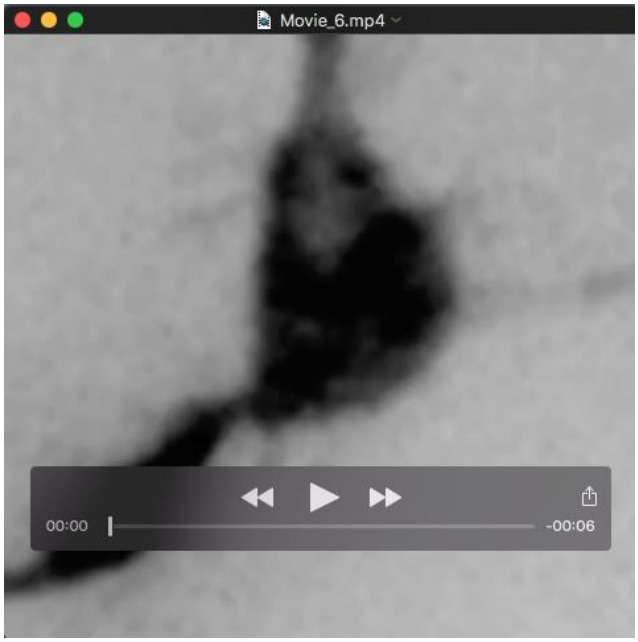

Movie 6. Representative *ttkRNAi*-expressing R7 axon terminal at 48 h APF. The average retraction velocity of processes is indistinguishable from that in wild type at 48 h APF; however, the average extension velocity of processes is greater than that in wild type at 48 h APF.